ELSEVIER

Solar Energy Materials & Solar Cells 60 (2000) 391–420

Solar Energy Materials & Solar Cells

www.elsevier.com/locate/solmat

Multicrystalline silicon solar cells with porous silicon emitter

R.R. Bilyalov[a,*,1], R. Lüdemann[a], W. Wettling[a], L. Stalmans[b], J. Poortmans[b], J. Nijs[b], L. Schirone[c,2], G. Sotgiu[c], S. Strehlke[d], C. Lévy-Clément[d]

[a]*Fraunhofer Institut für Solare Energiesysteme ISE, Oltmannsstrasse 5, D-79100 Freiburg, Germany*
[b]*IMEC vzw, Kapeldreef 75, B-3001 Leuven, Belgium*
[c]*Università Roma Tre, Via della Vasca Navale, 84, 00146 Roma, Italy*
[d]*Laboratoire de Physique des Solides de Bellevue, CNRS, UPR 1332, 1, Place Aristide Briand, 92195 Meudon CEDEX, France*

Received 9 February 1999; accepted 5 September 1999

Abstract

A review of the application of porous silicon (PS) in multicrystalline silicon solar cell processes is given. The different PS formation processes, structural and optical properties of PS are discussed from the viewpoint of photovoltaics. Special attention is given to the use of PS as an antireflection coating in simplified processing schemes and for simple selective emitter processes as well as to its light trapping and surface passivating capabilities. The optimization of a PS selective emitter formation results in a 14.1% efficiency mc-Si cell processed without texturization, surface passivation or additional ARC deposition. The implementation of a PS selective emitter into an industrially compatible screenprinted solar cell process is made by both the chemical and electrochemical method of PS formation. Different kinds of multicrystalline silicon materials and solar cell processes are used. An efficiency of 13.2% is achieved on a 25 cm^2 mc-Si solar cell using the electrochemical technique while the efficiencies in between 12% and 13% are reached for very large (100–164 cm^2) commercial mc-Si cells with a PS emitter formed by chemical method.

Keywords: Porous silicon; Multicrystalline silicon; Solar cell

* Corresponding author. Tel.: + 32-16-281545; fax: + 32-16-281501.
E-mail address: bilyalov@imec.be (R.R. Bilyalov)
[1] Present address: R.R. Bilyalov, IMEC, Kapeldreef 75, B-3001 Leuven, Belgium.
[2] Present address: Scuola di Ingegneria Aerospaziale, Università La Sapienza, Via Eudossiana 16, 00184 Roma, Italy.

0927-0248/00/$ - see front matter
PII: S0927-0248(99)00102-6

1. Introduction

A clear tendency towards simplified processing schemes with low thermal budget techniques is observable within contemporary crystalline silicon photovoltaic (PV) research. Selective emitter formation is considered as one of the possible ways to improve the crystalline silicon solar cell efficiency [1]. This step becomes especially important for the case of industrial screenprinted multicrystalline silicon (mc-Si) cells. In order to fabricate solar cells with screenprinted contacts two requirements should be fulfilled at the same time: a high surface concentration of the carriers under the contacts (in order to obtain a low contact resistance) and a deep n^+-p junction (in order to prevent shunts across the junction due to the diffusion of silver from the front contacts) [2]. However a straight forward application of such emitter results in a decrease of the short circuit current (I_{sc}) and the fill factor (FF). The only possible way to overcome these problems is to have an emitter with two distinct regions: a highly doped and deep region under the fingers and a lowly doped and thin one between fingers. Such an emitter structure can be realized using two diffusion and photolithography steps but this does not meet the industrial requirements. That is why a lot of effort is put in the field of simplified selective emitter processing. One of them is the so-called self-aligned emitter etch back process based on plasma [3] or chemical etching [2]. In both the cases an efficiency between 12% and 13% is achieved after applying conventional antireflection coating (ARC).

The recently proposed PS emitter concept based on chemical [4] or electrochemical etching [5] of the finished solar cells looks more attractive because it allows to form a selective emitter and an ARC in one step. Moreover PS has a potential to texturize [6] and passivate [7] the Si surface. Therefore the single step — formation of a selective emitter by converting part of it into PS — could simultaneously replace three other processing steps: texturization, passivation and ARC deposition. This makes this method of selective emitter formation more industrially applicable and therefore it needs to be investigated thoroughly.

First application of PS as an ARC for solar cells was made almost 15 yr ago [8] and since that time different research groups have tested PS material for photovoltaic devices [5,9–12]. All results point to an improvement of the optical characteristics due to the reduced reflectance losses of a PS surface. However sufficient PV characteristics are not yet obtained. The explanations are rather different: spreading resistance problem and charge trapping in PS [12], as well as high resistivity of interface PS-contacts [5] and surface recombination velocity [10]. The general characteristic is a non optimal solar cell design resulting in 9.2% efficiency as a maximum efficiency [10].

The first serious attempt to fabricate silicon solar cells with PS ARC is demonstrated in 1995. Both chemical [4,13] and electrochemical [14,15] methods are used for the formation of PS ARC on multi- and mono-Si solar cells. In the first case an efficiency of 10.4% for large area ($10 \times 10\ cm^2$) mc-Si solar cell with screenprinted contacts is obtained using a polymeric film for contact protection [13]. In case of the electrochemical approach for PS ARC formation an efficiency of 11.5% is reached without additional ARC deposition for the mc-Si cells with the same area and contacts [15].

Further research is to be done to bring the cells with PS ARC up to an industrially applicable level, first of all in term of efficiency. In order to increase these cell efficiencies up to 13–14% (industrial requirements) certain research work should be done. First of all some fundamental research is needed for a better understanding of the formation mechanisms and general properties of PS. Then some solar cells processing steps should be optimized in order to obtain an effective selective emitter, namely: emitter diffusion, metallization and PS ARC formation. Finally these research results should be incorporated in an industrial mc-Si solar cell fabrication process.

This work is currently in progress and all contributing research groups are involved. The main aim of this paper is to review our latest results on silicon solar cells with PS selective emitter. Some of these results are published for the first time. We will briefly describe the fabrication process of PS by both chemical and electrochemical method as well as structural and optical characteristics of the resulting PS. Then the main properties of PS ARC for Si solar cells will be discussed in detail. After that the results of the optimization of a PS selective emitter for silicon solar cells will be presented. And finally the current status of different screenprinted mc-Si solar cells with PS selective emitter will be outlined.

2. Porous silicon formation

In the beginning of the 1950s a lot of research was performed to employ chemical and electrochemical techniques to remove damaged surface material and/or to polish. In 1958 Turner [16] reported that Si is electropolished in hydrofluoric acid (HF) solutions if a critical current density is exceeded. Below the critical current density, a brown high-resistance film forms, which is, in historical perspective, the first report of PS formation. A few years later it was demonstrated that the chemical etching of Si wafers in HF/HNO_3 aqueous solution without applying any bias results in the formation of porous layers, quite similar to PS obtained by electrochemical technique [17]. The porous Si material resulting from an HF/HNO_3 — based mixture is called stain-etched PS. Since that time the properties of PS are continuously investigated and recently were summarized in an extended review [18]. We will discuss the formation conditions and properties of PS from the viewpoint of the photovoltaic application.

2.1. Electrochemically etched PS

2.1.1. Electrochemical formation process

Normally, Si almost does not dissolve in HF. However, if a current flows through the interface between the crystal and the solution, electrochemical etching occurs. This dissolution is only possible when the current delivers positive charge carriers (holes) to the interface, which is the case if the Si wafer is the anode of the electrochemical process (so called anodization). If a high current density is applied, there are many holes at the surface and the Si dissolution is limited by the diffusion of fluorine ions, which results in a smoothing of the surface (electropolishing). In the case of a low

current density, etching is limited by hole diffusion and the pits at the surface will be enlarged to form pores (porous etching).

The anodization is usually performed in an especially designed single compartment Teflon cell, using a two-electrode arrangement. The back of the Si wafer is held strongly to a metallic plate, often using a primary vacuum. The PS formation process is performed under galvanostatic control, i.e. a constant current density, which is obtained by regulating the voltage across the two electrodes connected to the potentiostat. The metallic plate acts as the working electrode while the counter electrode consists of a platinum wire which is positioned in the electrolyte above the Si surface which is to be etched. The ohmic contact to the back of the Si wafer as well as the sufficient conductivity within the wafer and the electrolyte ensure that the potential drop exists predominantly across the Si/electrolyte interface. In most cases the electrolyte consists of a mixture of HF and ethanol, in which the ethanol acts as a wetting agent.

Mesoporous structures with typical dimensions of 10–100 nm result from porous etching of degenerately-doped p- and n-Si. Hence the porous material which is formed at the n^+-Si emitter surface in solar cells belongs to this category.

2.1.2. Empirical formation rate and resulting morphology

Understanding of the porous silicon formation process and morphology (i.e. the porous layer thickness and porosity evolution with time) is essential in order to interpret the porous Si optical and surface passivation properties. From the solar cell point of view, particular interest exists in the porous morphology if part of the n^+-Si emitter surface is electrochemically etched. For this purpose, porous layers have been formed on uniformly doped n^+-Si emitter structures (realized by chemical vapour deposition (CVD)) as well as on diffused emitters, having a typical doping profile. CVD-emitter has been proven to be a useful tool to study the formation process because of the independent control of emitter doping level and junction depth.

In the case of a uniformly doped emitter, the thickness of the porous silicon layer increases linearly with the formation time as long as the layer thickness is significantly less than the junction depth. The formation rate decreases if the layer thickness approaches the junction depth which is understood as due to a collection of positive charge carriers by the base which competes with the PS formation. The formation rate decreases with increasing emitter doping level as shown in Fig. 1. Spectroscopic ellipsometry (SE)analysis on the other hand reveals a higher porosity when increasing the emitter doping level [19]. This increase in formation rate is linked to the porosity decrease through the electrochemical porous silicon formation which is performed under galvanostatic control. The porous silicon formation process is described as a process for which the dissolution of one Si-atom (in the porous etching regime) goes ahead with the exchange of two electrons in the external circuit. Hence applying a certain formation time, at a fixed current density, will in all circumstances lead to the same number of dissolved Si-atoms. At a constant current density, the porous layer thickness will therefore increase slowly in the case of high porosity since more Si-atoms need to be dissolved to obtain a certain porous layer thickness. As a result, in

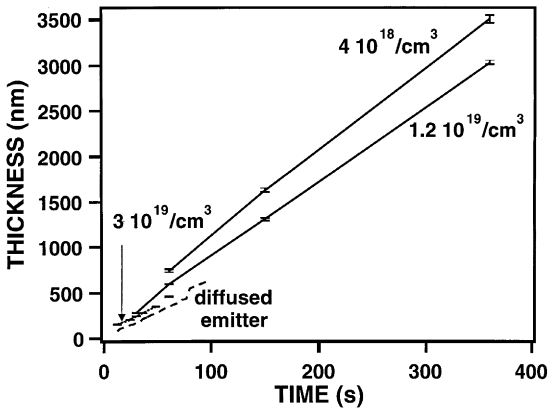

Fig. 1. Formation time dependence of the total layer thickness for various doping levels of the n^+-CVD layer. The initial thickness of the CVD layer is 5 μm, unless indicated otherwise. The data for the diffused emitter are added for comparison.

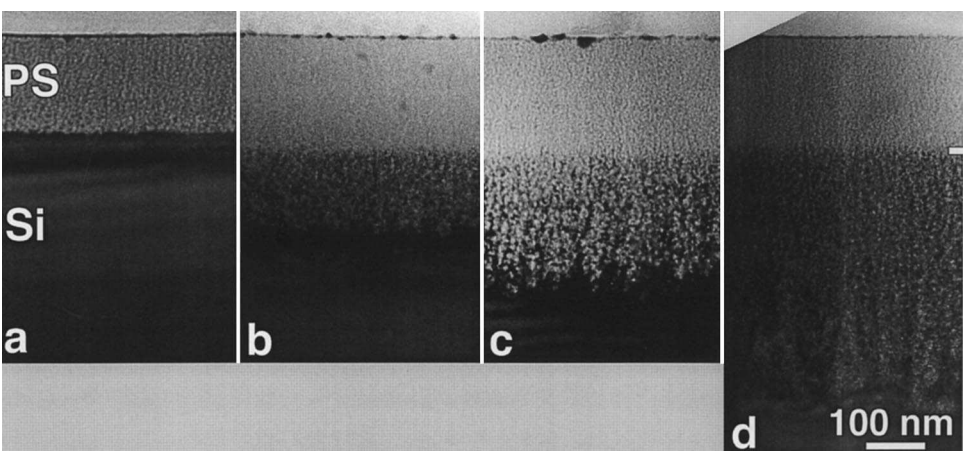

Fig. 2. XTEM-images of the PS layer grown on the diffused emitter for (a) 30 s; (b) 60 s; (c) 72 s and (d) 96 s.

the case of a diffused emitter, the continuously changing emitter doping level gives rise to a porosity gradient (Fig. 2) which on its turn slightly affects the empirical porous Si formation rate. The observations remain valid in the case of multicrystalline Si, except for an increased spread on the averages, which reflects the fact that the porous Si formation process exhibits some grain dependent properties.

2.1.3. Optical properties of anodically etched PS

A typical ARC behaviour is observed, with interference fringes and a number of extremes which increases with layer thickness. Fig. 3 illustrates the effect of an

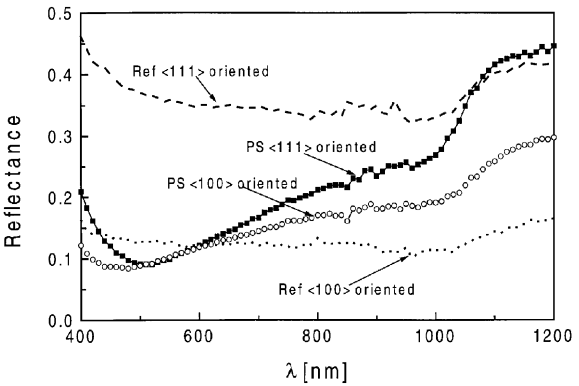

Fig. 3. Total reflectivity as a function of wavelength measured on the two ⟨1 0 0⟩ and ⟨1 1 1⟩ oriented grains of an n^+-p multicrystalline Si junction without a PS layer (Ref) and with a PS layer (PS).

electrochemically etched porous layer on differently orientated grains (⟨1 0 0⟩ and ⟨1 1 1⟩) after alkaline texturization. In both cases the presence of the porous layer introduces a "single-minimum" reflectance behaviour, which is typical for an ARC. Whereas for a textured ⟨1 0 0⟩ grain the total reflectance remains virtually the same after porous Si formation, the total reflectance significantly reduces in the case of a textured ⟨1 1 1⟩ grain. Hence the presence of a porous Si layer partially works away the differences in reflectivity which exist from grain to grain on multicrystalline materials after an alkaline texturization.

The crystallographic orientation of various grains of the wafer is deduced from the morphology of their surface after NaOH texturization, observed using scanning electron microscopy (SEM). The surface microstructures of two ⟨1 0 0⟩ and ⟨1 1 1⟩ oriented selected grains are characterized by the presence of pyramids and flat triangles, respectively [20]. Fig. 3 shows the total reflectivity (R) as a function of wavelength for the two grains with and without a PS layer. Due to the presence of the pyramids which are known to trap efficiently the light, the reflectivity of the ⟨1 0 0⟩ grain without a PS layer is much lower than the one of the ⟨1 1 1⟩ oriented grain whose texturized surface exhibiting flat triangles does not trap the light at all. The presence of a PS layer slightly modifies the reflectivity of the ⟨1 0 0⟩ grain, whereas it dramatically decreases the reflectivity of the ⟨1 1 1⟩ grain. The integral reflectance, R, defined as:

$$R = \int_{400}^{1100} R(\lambda) J_0(\lambda) \mathrm{d}\lambda \Big/ \int_{400}^{1100} J_0(\lambda) \mathrm{d}\lambda,$$

(with R the reflectivity and J_0 the solar flux under AM 1.5 standard conditions) are reported in Table 1 for the two grains. The smallest calculated effective reflectance is obtained for the ⟨1 0 0⟩ grain, subjected to a NaOH texturization only, whereas surprisingly the presence of a PS layer slightly increases R_{Eff}. In the case of the ⟨1 1 1⟩

Table 1
Effective reflectivity for the ⟨1 0 0⟩ and ⟨1 1 1⟩ grains with and without a PS layer

	⟨1 0 0⟩ oriented grain		⟨1 1 1⟩ oriented grain	
	Ref	With a PS layer	Ref	With a PS layer
Effective reflectivity %	12.4	15	35.5	19

grain addition of a PS layer dramatically decreases the reflectivity from 35.5% to 19% without and with PS, respectively. Therefore electrochemical etching results in the decrease of the initial difference between ⟨1 0 0⟩ and ⟨1 1 1⟩ oriented grains and leads to the formation of an uniform ARC layer on a textured multicrystalline Si surface [21].

The porous Si layer with a certain range of thicknesses (100–160 nm) on top of the cell structure absorbs a part of the incident light. Due to the porous morphology and its observed high electrical resistivity, the photogenerated carriers are considered to be lost (because of recombination before they can reach the underlying active solar cell). As a result, the part of the incident light which is absorbed in the porous layer does not contribute to photogeneration in the active solar cell. This absorption in the PS layer gives rise to a current loss of approximately 0.5 mA/cm^2 for a PS with a thickness (80–100 nm), which is optimal for ARC purpose.

2.2. Stain etched porous Si

At present it is generally accepted that chemical etching of Si surface in HF/HNO_3 based solution can be considered as a localized electrochemical process. The silicon surface is oxidized by hole injection from HNO_3 and then it is etched by a reaction with HF in a similar way as it is done in the electrochemical process. The overall chemical reaction on the Si surface can be described as:

$$3Si + 4HNO_3 + 18HF \rightarrow 3H_2SiF_6 + 4NO + 8H_2O + 3(4-n)h^+ + 3(4-n)e^-,$$

where n is the average number of holes required for dissolution of one Si atom [22]. The main difference between these two techniques is that stain etching is a self-regulating process and strongly depends on the initial solution content. In the stain etching process HNO_3 plays the same role as the anodic current density in the electrochemical one. That means that an HNO_3 -rich chemical mixture corresponds to the high-current regime in the electrochemical dissolution while an HF-rich solution results in a process that is limited by the availability of holes and gives rise to stain etching corresponding to the low-current regime in the case of electrochemical process. That is why the HNO_3 content in the starting solution is the most important parameter for stain etching. Other parameters affecting the stain etched PS properties

are the following: duration, illumination and temperature during the process, doping level and morphology of the initial Si surface.

2.2.1. Structural properties of stain etched PS

Electron microscopic observations show that stain etched PS is quite similar to anodical PS but with some distinct differences [23]. Cross sectional Transmission Electron Microscopy (TEM) micrographs in Fig. 4 show that the PS layers are typically characterized by a graded transition from bulk to a shallow high porosity region, with single crystalline Si filaments, embedded in a low density amorphous matrix [24]. The HREM observations show that very different morphologies can be obtained, changing HNO_3 content and etching time. PS was prepared on a polished $\langle 1\,0\,0 \rangle$ Si surface, under different formation conditions. As can be seen from Fig. 4, the difference between single crystal domain dimensions may achieve an order of magnitude and strongly depends on formation conditions. An increasing of HNO_3 content leads to the decrease of microcrystallities and an increase of pore size. As a result, the PS prepared in the solution with the highest nitric acid concentration shows a sharp transition between the bulk and a highly wide porosity region, while

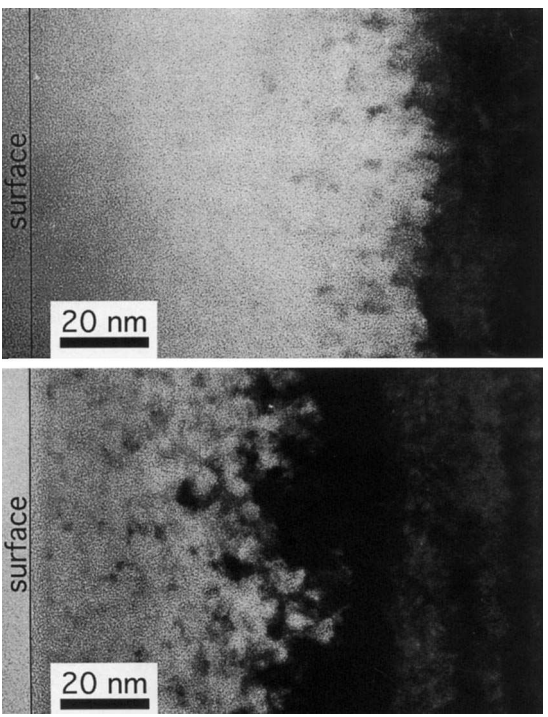

Fig. 4. Cross sectional TEM micrographs of stain etched PS, prepared in a different condition: top — 17 s, $HNO_3 = 0.024$ mol/l; bottom — 55 s, $HNO_3 = 0.006$ mol/l. Experimental measurements were taken every 10 nm, and the surface lines are mere guidelines for the eye.

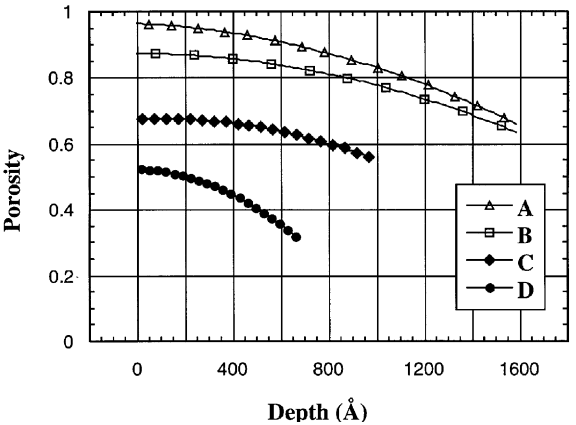

Fig. 5. Porosity profiles for different formation conditions: (A) textured substrate, $HNO_3 = 0.048$ mol/l, $t = 20$ s; (B) textured substrate, $HNO_3 = 0.024$ mol/l, $t = 50$ s; (C) polished $\langle 1\,0\,0 \rangle$ substrate, $HNO_3 = 0.024$ mol/l, $t = 17$ s; (D) polished $\langle 1\,0\,0 \rangle$ substrate, $HNO_3 = 0.006$ mol/l, $t = 55$ s;

when a lower concentration of HNO_3 are used in the solution, a rather smooth transition is observed.

This fact is fully confirmed by porosity profiles of the PS layers as plotted on Fig. 5 for different formation conditions. The porosity is deduced from reflectance spectra by the Bruggemann Effective Medium Approximation describing PS as composed of crystalline silicon and air [25]. The air volume fraction (i.e. the porosity) is zero in the bulk and increases towards the film/air interface. As follows from Fig. 5, the increase of HNO_3 content results in an increased porosity. Moreover, it is clearly seen that the PS formation rate is proportional to the concentration of nitric acid in the solution. Increase of HNO_3 content by four times results in an increase of growth rate by almost two times. This means that an appropriate growth rate of PS can be obtained in stain etching process by choosing a certain chemical solution. Therefore PS with a wide range of properties can be obtained by stain etching: porosity from 20% to 100% and the thickness from a few nm to hundreds nm.

2.2.2. Optical properties of stain etched PS

Optical properties of stain etched PS are also strongly dependent on the etching process parameters: chemical solution, duration, temperature and illumination. In order to reduce the number of parameters, all experiments described in this paper are carried out at room temperature and under laboratory background illumination. In the case of stain etching it is difficult to separate the effect of chemical composition and duration of the process on PS characteristics, since the nitric acid concentration in the chemical solution affects both the porosity of PS as well as the formation rate of PS. Therefore the most important technological parameter should be a function of the chemical composition as well as of the process duration. This is the so-called Ct parameter, where C is the HF/HNO_3 ratio and t is the etching time [4,26]. This

technological parameter allows to set the PS layer thickness to a fixed value independent of the process [24].

The reflectance characteristics of mc-Si wafers with PS prepared by stain etching for various Ct parameters are depicted in Figs. 6 and 7. Fig. 6 shows the reflectance characteristics of PS prepared by etching in different solutions for a fixed time, while Fig. 7 shows the reflectance characteristics of PS etched for different durations a fixed solution. As follows from the reflectance characteristics, the duration of the etching affects the location of the minimum of the reflectance, while the HNO_3 content mainly affects this minimum value [24,26].

The refractive index of PS depends on its porosity. However, as stated in the previous section, the porosity of PS has a gradient in depth and it is very difficult to determine exactly the refractive index of PS, especially in the case of multicrystalline

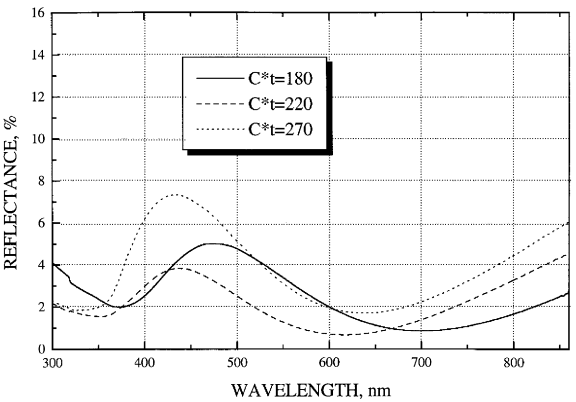

Fig. 6. Reflectance characteristics of PS layers resulting from three different preparation conditions given by the Ct parameter, where t = Const.

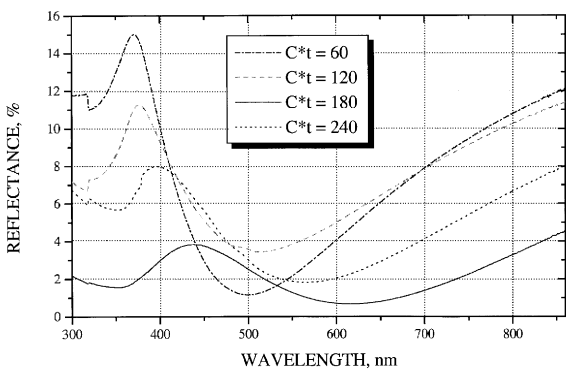

Fig. 7. Reflectance characteristics of PS layers resulting from three different preparation conditions given by the Ct parameter, where C = Const.

Si. Variations of the refractive index are possible in the range of 1.5 to 2.2 depending on the *Ct* parameter, as it shown in [26].

3. Porous silicon in solar cell processing

3.1. Major properties of PS ARC

Improved light trapping and a lower surface recombination velocity are crucial for crystalline Si cell structures with thin active regions. A PS layer on top of a Si solar cell might act as an ARC because of its refractive index which depends on the porosity and morphology and which can be close to the optimal one of an ARC for Si solar cell. Furthermore, the incoming light might be scattered due to interaction with PS structure. Finally the PS structure generally is assumed to give rise to quantum confinement and an increased bandgap. The wide bandgap of PS might be useful to establish a minority carrier mirror, which could contribute to surface passivation. Therefore a well-founded judgement about PS benefits in such cell structures requires a detailed investigation of both the light diffusing behavior and surface passivation capabilities of PS.

3.1.1. Light diffusing behavior of PS ARC

A significant increase of the internal quantum efficiency (IQE) in the long wavelength range (red response) is observed when a porous surface layer is present on top of a conventional silicon solar cell structure (Fig. 8) [27]. A linear relation exists between the measured IQE and the absorption depth ($1/\alpha$), in which the slope is determined by both the entrance angle (θ) of the light entering the cell structure and the effective bulk diffusion length L_{eff}. An "effective" entrance angle of 60° is found for the light entering the cell structure after passing through a 160 nm porous surface

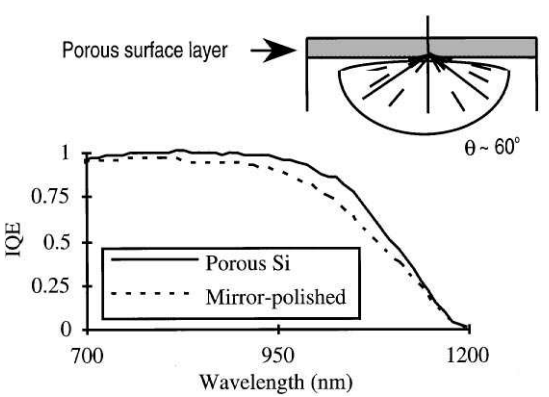

Fig. 8. Measured IQE-data for conventional cell structures with a mirror-polished and a porous top surface. The increase of the IQE in the 800–1000 nm wavelength range is attributed to the light diffusing behaviour of PS.

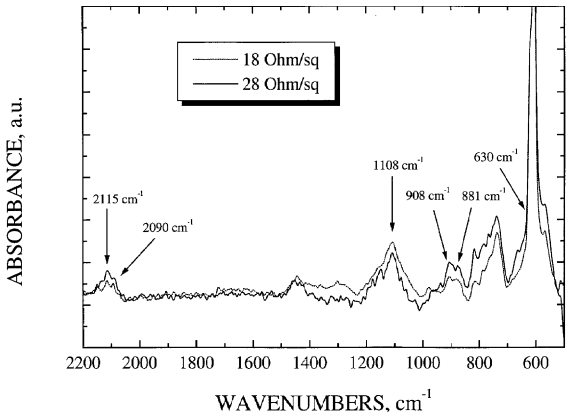

Fig. 9. FTIR-spectra of mc-Si samples with different R_s covered by stain etched PS. (18 Ω/□ — dotted line; 28 Ω/□ — solid line)

layer, which means that the light is fully randomized due to the scattering behaviour of the random PS medium (Fig. 8). This difference in entrance angle for the mirror-polished and porous Si surface cell explains the significant change in IQE. Due to the light-diffusing behaviour of porous Si, more light is absorbed closer to the p–n junction. This results in a higher collection efficiency and hence an increased internal quantum efficiency. It should be noted that this light diffusing property of PS depends on the PS layer thickness and is less pronounced for an optimal PS ARC layer (80–100 nm) [28].

Recently a model for light propagation in porous silicon has been developed [29] based on the random-medium theory. The specular and the diffuse part of the light can be determined and treated separately. This analysis points to a scattering behaviour which is stronger in the forward direction, i.e. transmission, than in the reverse way, i.e. reflection. In this way the modelling is consistent with the experimental observation of a rather specular reflectance behaviour in combination with a light diffusing action for the transmitted light.

3.1.2. Surface passivating capabilities of PS ARC

It is well known that a large number of Si-hydrides as well as Si-hydroxides forms during PS growth [23]. Some of them can quite well passivate the Si/PS interface. The typical Fourier transform infrared (FTIR) spectra of n^+-p mc-Si samples with initial sheet resistance (R_s) of 18 and 28 Ω/□ covered by stain etched PS are plotted in Fig. 9. Most of the peaks are the same as observed for electrochemical PS. The identification of the peaks is given elsewhere [30]. The intensity of the Si–H stretching mode in the stretch region (2100 cm^{-1}) shows the quality of passivation. This stretch hydrogen signal is quite comparable to Si–H signals of bending region (630 cm^{-1}) that means that the Si surface can be relatively well passivated after PS formation. This claim has been checked by microwave-detected photo-conductivity (PCD) analysis (Fig. 10) [31]. The whole surface of a 10×10 cm^2 mc-Si wafer is tested in 100 points before and

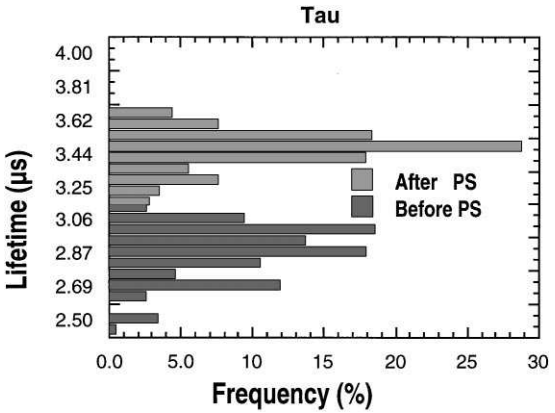

Fig. 10. PCD-analysis of lifetime of stain etched PS using a 523 nm laser illumination and microwave detection at 13.56 MHz [29].

after PS formation. It should be noted that the lifetime (τ_{eff}) measurement of the sample with a PS surface is carried out approximately 1 month after the PS formation. This result shows that a slight improvement of τ_{eff} ($\sim 20\%$) remains after an air exposure for a long time.

The same technique has been applied to derive the effective minority carrier lifetime for an electrochemically formed PS on a mono-Si surface. Immediately after PS formation, τ_{eff} is significantly higher when porous surface is present, but it has to be stressed that a comparison is made with an unpassivated surface of which the surface recombination velocity approaches the thermal velocity 2×10^7 cm/s (Fig. 11). After that τ_{eff} exhibits a certain degradation during ageing in ambient and after a few days shows nearly the same relative improvement as in the case of stain etched PS. In both cases a PCD analysis clearly indicates that PS has some passivating capabilities which need to be improved by further optimization of PS formation or by external treatments.

Therefore different PS treatments [32,33] have been investigated with the aim of maintaining the light diffusing property while both the absorption losses are reduced and surface passivation is improved and stabilized. Rapid thermal oxidation (RTO), nitridation and anodic oxidation have been selected as potentially interesting pathways to chemically modify the electrochemically formed PS with a low thermal budget in common.

3.1.3. Low-thermal-budget treatments of electrochemically etched PS

Oxygen is incorporated in PS when stored in ambient (ageing) giving rise to the uncontrolled presence of suboxides, approaching a SiO_2 stoechiometry in the outer region. This leads to an unstable surface passivation of a porous surface layer in a crystalline Si solar cell and a recombination velocity of approximately 5×10^5 cm^2 as extracted from IQE data [27]. Furthermore some light is lost due to absorption in

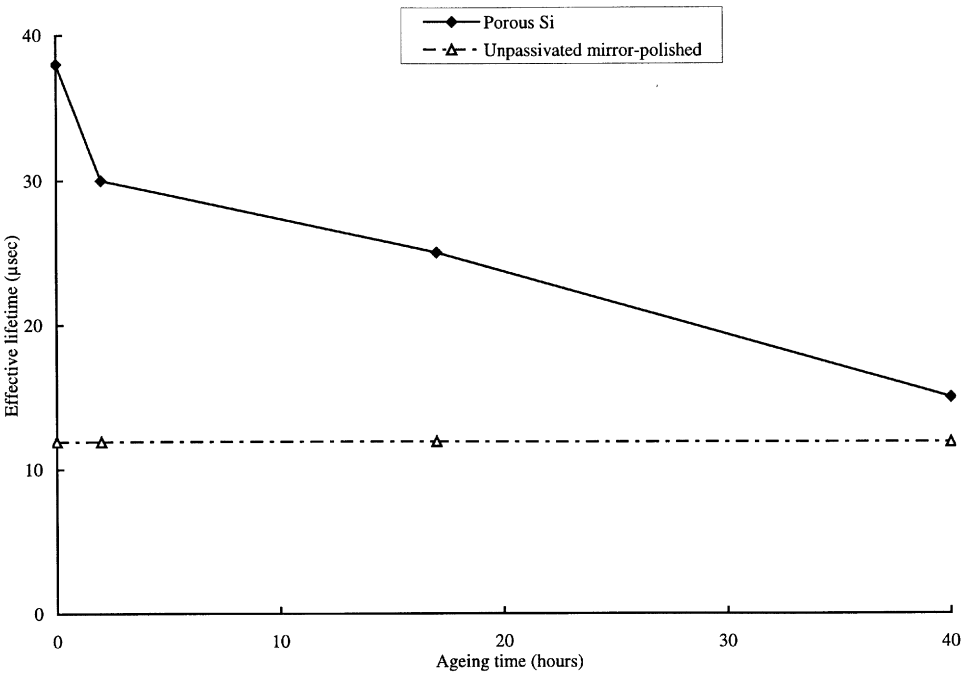

Fig. 11. PCD-analysis of lifetime of electrochemically etched PS using a 1047 nm laser illumination and microwave detection at 22 MHz [26].

the porous layer. Anodic oxidation gives rise to the uniform presence of a silicon oxide layer on the pore walls while the porous structure remains largely intact. On the solar cell level however, this PS modification technique does not result in a pronounced improvement of the blue response while the red response remains unaltered.

Rapid thermal oxidation of PS converts the material into a low-porosity SiO_2. This mixed-medium structure still gives rise to light diffusion of the transmitted light. Light absorption is virtually absent in this oxidized surface layer. No improvement of the surface passivation is observed for RTO treatments except for temperatures $> 950°C$. This passivation effect originates from a simultaneous oxidation of the Si bulk underneath which leads to the creation of an intermediate oxide at the PS/Si interface.

The plasma nitridation of PS is able to incorporate nitrogen uniformly throughout the porous layer while preserving its porous nature. The effects of the nitridation are not limited to the PS surface atoms only, but also affect the inner Si-atoms. The effects of rapid thermal oxidation and nitridation on PS structure are shown in Figs. 12 and 13.

In all the three cases, important drawbacks are the presence of an additional process step as well as the fact that the refractive index decreases which is unfavourable from the viewpoint of ARC-properties. One might compensate this decrease in refractive index by increasing the initial PS refractive index through a lower porosity.

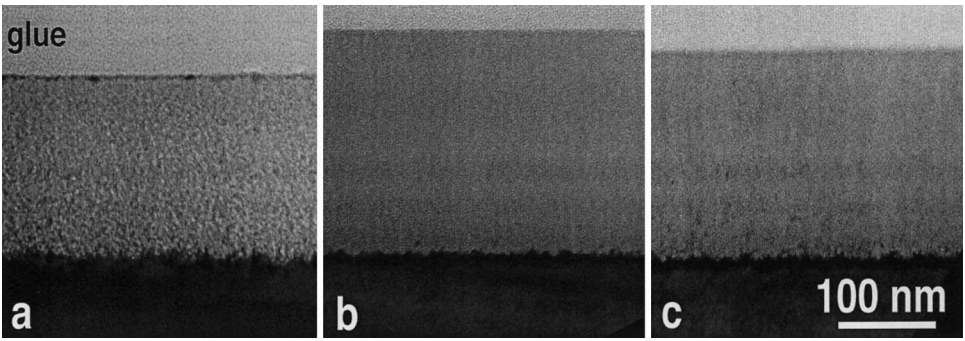

Fig. 12. XTEM of: (a) initial PS; (b) a porous layer after RTO (850°C; 30 s) and (c) after RT nitridation.

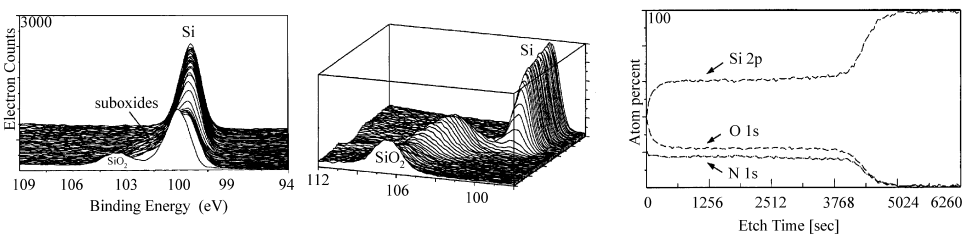

Fig. 13. (A) XPS spectra of PS recorded after different etch times, revealing SiO_2 in the outer region (peak at 103.5 eV) and the presence of suboxides in the inner region (shoulder to the 99.9 eV Si-peak); (B) XPS spectra (97–112 eV) of PS after RTO (850°C — 60 s) recorded after different etch times, revealing a pure SiO_2 spectrum and the elemental Si peak of the underlying Si substrate; (C) XPS depth profile of DP-nitrided PS.

However lowering the porosity is directly linked with a decreased internal surface area and hence a lower reactivity of the porous material.

3.2. Optimization of mc-Si solar cells with porous Si selective emitter

3.2.1. Cell processing sequence

As mentioned already, a significant research effort was put into the search for a simple porous etch to obtain simultaneously an effective ARC and a selective emitter structure [26,34–36]. Both the chemical and electrochemical formation methods are currently under investigation by different research groups because no clear-cut arguments to decide on one or another technique are now available [37]. The typical process sequence results in a selective emitter structure because PS is formed after front-side metallization. A general tendency throughout the results is an increased J_{sc} due to the reflectivity reduction by PS ARC. The V_{oc} of such cells can slightly increase or decrease depending on initial emitter structure. As a result an efficiency around 13% is reported for the pre-textured cells with non-optimal PS emitter

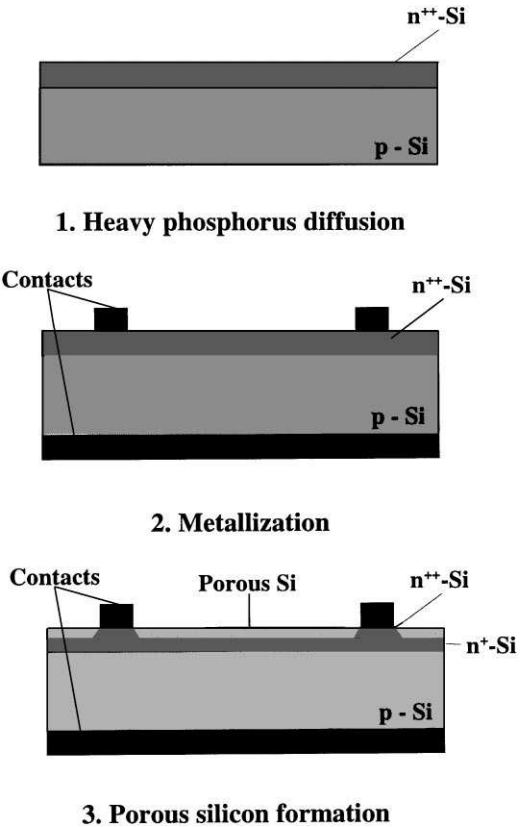

Fig. 14. Solar cell process sequence for PS selective emitter formation.

structure. One of the advantages of PS formation is the possibility of simultaneously texturizing the Si surface [30,38,39] and therefore texturization can be skipped in the cell processing. Passivation capabilities of PS has been already discussed and as it follows from Section 3.1.2., PS layer provides slight passivation which is quite enough for mc-Si material, because the characteristics of mc-Si solar cells are mainly determined by the quality of bulk of mc-Si material. As shown in Fig. 14, the process sequence for fabrication of solar cell with PS selective emitter is much simpler than the conventional one.

There are a number of advantages of such selective processing:

- Heavy and deep phosphorus diffusion is beneficial for impurity gettering.
- The surface is uniformly textured after n-p junction formation.
- No surface passivation is applied.
- No additional ARC deposition is required.

To realize a strongly simplified processing scheme, two main requirements are put forward: (i) optimize the PS layer to replace the conventional texturization, passivation and ARC deposition and (ii) optimize the initial emitter in order to avoid losses in I_{sc} and V_{oc}.

3.2.2. Optimization of PS layer

In the optimization experiments the chemical PS formation method was used because of its simplicity and effectiveness. The most commonly used solutions for formation of stain etched PS are $HF/HNO_3/H_2O$ and $HF/HNO_3/CH_3COOH$. Acetic acid and water basically do not participate in the reaction except for reducing/increasing the main reactant concentration. Also acetic acid wets silicon surface, but in the case of a surface with many defect sites (mc-Si material) on which the chemical reaction is started, it is not necessary to have a wetting ingredient in a solution. Therefore the aqueous solution is choosen because of cost considerations. The optimization of the HNO_3 content in the chemical solution leads to the formation of a microstructure on the surface for all kinds of mc-Si materials with macroelevations covered by a nanoporous layer as it occurs by acid texturization [38,39].

The Si surface textured in such a way has a very low reflectance, quite comparable to with reflectance of an alkaline textured Si covered by double-layer ARC. These reflectance characteristics are plotted in Fig. 15. The integral reflectance in the wavelength range 300–1000 nm is decreased after etching from 38–39% to 5–6% depending on the type of mc-Si materials. The optimal PS providing the best reflectance is found to have a thickness of about 100–120 nm, a porosity of about 65% and a refractive index of about 1.9. The stain etching process for such PS formation is

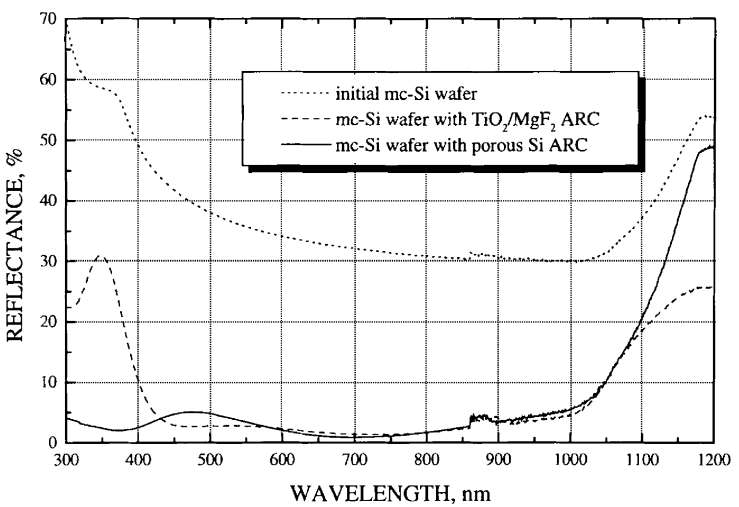

Fig. 15. Reflectance characteristics of non-textured mc-Si wafer after PS formation and pre-textured mc-Si wafer with double layer ARC.

characterized by *Ct* equal to 120. More detailed information concerning the optimal stain etching process can be found elsewhere [40]. A comparison of the optimal PS ARC formed on non-textured mc-Si surface and conventional double-layer ARC formed on alkaline textured mc-Si surface shows some advantages of the first one. First of all, stain etched PS is formed uniformly on the whole area of the mc-Si wafer almost independently of the grain orientation, while conventional alkaline texturing only works well in the case of mono-Si. Secondly, the reflectance of stain etched PS is significantly higher in the infrared region (which avoids the detrimental heating of the cell) and significantly lower in the short wavelength region.

As has been shown in Section 3.1.2., at certain conditions PS layer can provide slight passivation of the surface. As follows from Fig. 10, the hydrogen signal from both stretch and bending regions is significantly lower in the samples with highly doped emitter. PCD analysis shows a slight increase of effective lifetime that probably can be improved by further optimization [41].

Taking into account the light diffusing behavior of PS, it can be concluded that PS with the optimal thickness, porosity and refractive index provides an excellent reflectance and appropriate passivation for all kinds of mc-Si materials [30]. Therefore PS layer at certain conditions could replace three conventional technological steps in solar cell processing: texturization, passivation and ARC deposition.

3.2.3. Optimization of selective emitter

Rather high emitter doping levels are applied industrially, normally resulting in the presence of a dead layer at the emitter surface. Light absorbed in this region is considered to be lost because photogenerated carriers will recombine before being collected by the p–n junction, due to the small diffusion length associated to high doping levels [27]. The conversion of the highly doped region between the finger contacts into PS results in a lower surface concentration, but such an emitter requires a very effective passivating layer (more effective than provided by existing PS). Another emitter parameter, the thickness, should be optimized as well taking into account the following facts: the initial emitter should be rather thick in order to allow PS formation and screen printed contacts. On the other hand, such an emitter should be rather thin to provide an appropriate value of J_{sc}. The establishment of the compromise between doping profile and the thickness of the emitter is the main goal of the PS selective emitter optimization.

The optimization of the initial emitter is started by an optimization of the doping level. With this aim 16 groups of the cells with different sheet resistance are fabricated using a post-diffusion etch-back process [26]. Then PS layers are formed by stain etching under optimal conditions, as discussed in the previous section. The distribution of J_{sc} as well as the increment of J_{sc} after PS ARC formation as a function of emitter sheet resistance are plotted in Fig. 16. This first test indicates that R_s of the initial emitter should not exceed 35 $\Omega/\square$ in order to obtain an appropriate value of the J_{sc}.

Further optimizations are made using the electrochemical C–V technique [30]. PS is formed on the mc-Si samples with deep and highly doped emitters with three different R_s: 18–20, 28–30, and 33–35 $\Omega/\square$. The carrier concentration profiles before

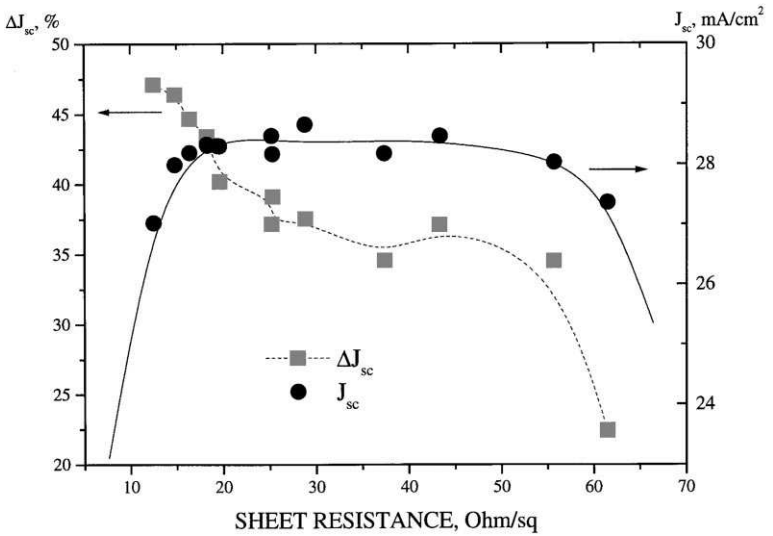

Fig. 16. J_{sc} and increment in J_{sc} of the cell after PS ARC formation in dependeing on emitter sheet resistance.

and after PS formation are presented in Fig. 17. In order to obtain the desirable value of an R_s of no more than 100 Ω/□ for the finished thick emitter (with PS),the R_s of the initial emitter (without PS) should not exceed 30 Ω/□. The optimum for mc-Si solar cells with PS selective emitter is found to be a sheet resistance 100 Ω/□ and a thickness of 0.65 μm. Such an emitter provides a highly doped region under the contacts and an optimal carrier concentration in between the fingers such that no additional passivation is required. The thickness of such an emitter allows to fire screenprinted contacts, to have a high V_{oc} and simultaneously to avoid losses in J_{sc} due to absorption of the free carriers.

3.2.4. Solar cells with an optimal PS selective emitter

The solar cells with an area of 5×5 cm^2 are fabricated on non-textured wafers from three different mc-Si materials by a very simple technology, consisting of three main steps, as it shown on Fig. 14. After formation of a deep and highly doped n^{++} emitter layer with the resistivity of 28 Ω/□ by thermal phosphorus diffusion, wafers are metallized by evaporation of Ti/Pd/Ag contacts on the front and Al on the back-side. In order to improve the quality of mc-Si materials, all samples are hydrogenated by remote plasma technique, which has been found as a most effective method of bulk passivation of mc-Si [42]. After that the cells are etched in HF/HNO_3 aqueous solution for a few seconds to form PS selective emitter as described in [40].

The *I–V* characteristics of these cells are plotted in Fig. 18. The efficiency of the cells shows the dependence on initial quality of mc-Si material. The solar cell with a PS selective emitter fabricated on mc-Si Eurosolare demonstrates a high efficiency as compared to those of Baysix and EMC materials.

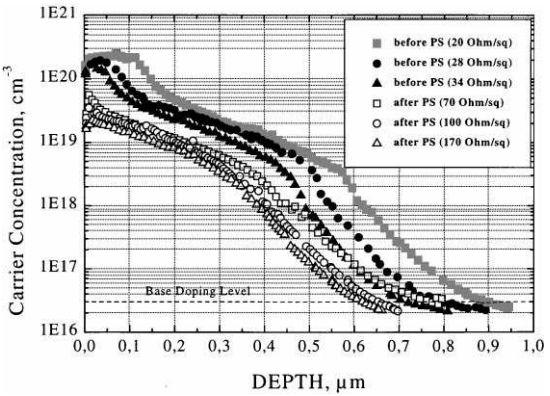

Fig. 17. Carrier concentration profiles of the emitters with different R_s before and after PS formation.

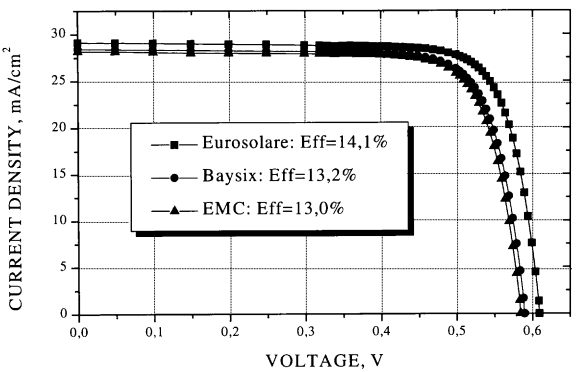

Fig. 18. *I–V* characteristics of solar cells with PS selective emitter proceeded on the different mc-Si materials under AM 1.5 spectrum as measured at Fraunhofer-ISE [28].

The output PV parameters of these solar cells are summarized in Table 2. Optimization of the PS formation conditions and initial emitter parameters results in a J_{sc} increase of almost 40%, as well as a V_{oc} increase of about 4–6 mV. Absolutely no degradation of front contacts and FF is observed, although the cells are not protected during stain etching.

The efficiency of 14% on the mc-Si (25 cm^2) cell with a PS selective emitter without applying texturization, passivation or an additional ARC deposition shows the large potential of PS in silicon solar cell technology.

3.3. Screen printed mc-Si solar cells with PS emitter

As was shown in the previous section, the efficiency of 13–14% for the mc-Si solar cells with a PS emitter fabricated by a very simple technology (without texturization,

Table 2
PV output parameters of $5 \times 5\ cm^2$ mc-Si solar cells with PS selective emitter as measured under AM 1.5 spectrum

mc-Si material	J_{sc} (mA/cm^2)	V_{oc} (mV)	FF	EFF (%)
Eurosolare	29.13	609.3	0.797	14.1
Baysix	28.45	590.0	0.789	13.2
EMC	28.19	584.4	0.788	13.0

BSF-formation, surface passivation and additional ARC deposition) gives hope that this cell design could be successfully applied in commercial cells. However, in order to meet the industrial requirements, PS ARC should be fabricated on the large-area mc-Si cells with screenprinted contacts. Ag-screenprinted contacts are more degraded after exposure in HF-based solution than Ti/Pd/Ag evaporated ones. Both chemical [43,44] and electrochemical [20] methods of PS formation were successfully applied for commercial cells. Each method has some advantages and drawbacks from the viewpoint of industrial application. The electrochemical method allows a better control while stain etching is more suitable for large scale production. Since no clear arguments for one or another techniques are available, the results on the implementation of both methods in industrial mc-Si cell processing are presented in the next sections.

3.3.1. Chemical method

Two research groups independently try to implement stain etched PS ARC into the screen printing process currently used in PV industry. A group from Università Roma Tre (RM3) worked on the cells from Eurosolare S.p.A. [43] whereas a group from Fraunhofer-ISE (ISE) [44] worked on commercial cells from ASE GmbH.

3.3.1.1. Experimental. Solar cells used at RM3 are fabricated on the basis of the screen printing process currently used at Eurosolare S.p.A.. Multicrystalline Si wafers (Eurosolare) with an area of $12.5 \times 12.5\ cm^2$ are previously textured in KOH. No BSF is present. The sheet resistance of the initial emitter was nearly 30 $\Omega/\square$. Silver contacts are deposited both on the front and on the rear side by screen printing and eventually protected by a polymeric film, which is also deposited by screen printing. The solar cells are dipped in aqueous solutions containing $HF : HNO_3$ in a ratio of the order of 1000 : 1. The PS thickness is set to minimize the integral reflectance (R). Finally the protective film is removed in aceton.

All experiments at ISE are carried out on $10 \times 10\ cm^2$ commercial mc-Si solar cells with screenprinted contacts produced by the standard technology of ASE GmbH. The initial non-textured mc-Si wafers (Baysix) are p-type, boron doped with a resistivity of about 1 Ω cm and a thickness of 350 μm. After the ASE standard process, PS ARC is formed on fully metallized cells without any protection by stain etching under conditions as described in [40]. In both cases the process is self-aligning, as the

contacting grid is deposited before PS formation and the PS ARC is formed only on the uncovered silicon surface among the metal fingers.

3.3.1.2. Results. The output photovoltaic parameters under global AM1.5 illumination for the screenprinted solar cells produced by ISE and RM3 groups before and after PS formation are summarized in Table 3.

The main problem preventing the achievement of a higher efficiency on the ISE solar cells is the FF degradation after the PS ARC formation. The analysis of the dark I–V characteristics shows that this behaviour is related to the increase of the series resistance R_s, mainly due to the interaction of HF acid from etching solution with glass-containing Ag paste of screenprinted contacts [44]. The parameters from the dark I–V characteristics are calculated using the two-diode model and are summarized in Table 4.

In the RM3 cells the metallizations is protected by a polymeric film: this explains the smaller degradation of R_s and the achievement of larger FF [43]. On the other hand, the protecting film also screened a surface region as wide as 0.1 mm along the grid fingers against the etching solution: this region was not AR coated, causing the observed J_{sc} reduction with respect to ISE solar cells.

Another possibility is the combination of PS layer for selective emitter formation with standard screenprinted TiO_2 ARC. A 12.9% efficiency is obtained in these devices, where a thin PS layer (50 nm) is only used for etch-back and passivation, whereas TiO_2 layer provided the optical thickness required for the desired AR effect (Table 3).

Table 3
I–V characteristics of the screenprinted mc-Si solar cells before and after the PS ARC formation

Cells from	Process	PS ARC	Area (cm^2)	J_{sc} (mA/cm^2)	V_{oc} (mV)	FF	EFF %
ASE	ISE	No	100	22.3	575	0.774	9.9
ASE	ISE	PS	100	28.9	574	0.740	12.3
Eurosolare	RM3	No	164	22.4	588	0.685	9.0
Eurosolare	RM3	PS	164	27.2	592	0.753	12.1
Eurosolare	RM3	No	164	22.5	589	0.694	9.2
Eurosolare	RM3	PS + TiO_2	164	28.5	595	0.758	12.9

Table 4
Parameters of the model for dark I–V characteristics of the ISE solar cell

Cell	$J_{01} \times 10^{-12}$ (A/cm^2)	$J_{02} \times 10^{-7}$ (A/cm^2)	R_s (Ohm cm^2)	$R_p \times 10^3$ (Ohm cm^2)
Without PS	9.1	6.1	0.72	3.87
With PS	0.6	0.4	1.01	15.5

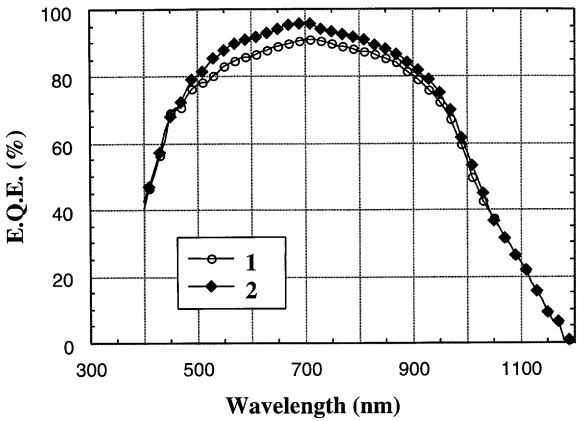

Fig. 19. EQE of PS-coated (1) and back etched (2) mc-Si solar cells.

In Fig. 19 the external quantum efficiency (EQE) curve for a RM3 PS-coated solar cell is reported in comparison to the EQE of a back etched (BE) solar cell. In the first device the shallow heavily-doped low-lifetime silicon layer is converted into the porous, low absorption material, while in case of BE this layer is completely removed. A single-layer TiO_2 film is used as an ARC for BE solar cell.

Very similar EQE are observed in the blue-violet spectral region, demonstrating the effective back-etching and passivating effects of PS layers. On the other hand, in the visible spectral region the PS-coated solar cell shows an appreciable EQE reduction, which can be ascribed to the non-optimized doping profile: the PS layer thickness is set after a compromise among separate R_{eff}, J_{sc} and V_{oc} optimizations [13,43], and the dead layer is not completely removed. The J_{sc} close to BE devices is expected to be achieved with a better matching between the ARC and the dead layer thicknesses. The J_{sc} and the effective diffusion length of the minority carriers, as calculated from the spectral response curves for the PS-coated and for the BE devices were 31.9 mA/cm^2, 193 μm and 33.2 mA/cm^2, 199 μm, respectively.

Fig. 20 shows the internal quantum efficiencies (IQE) as well as the reflectance characteristics of ISE solar cells with PS and double layer (TiO_2/MgF_2) ARC. In the wavelength range of 450–800 nm the IQE of the cell with PS ARC is higher than that of the reference cell, while the reflectance is nearly unchanged. This enhancement can be explained by the decrease of the surface carrier concentration after etching as well as by partial surface passivation by the PS ARC. The calculation of J_{sc} from integration of IQE gives the value of 31.8 mA/cm^2. The gap between experimental and extrapolated J_{sc} values could be reduced after optimization of process parameters.

As it has been shown in this section, PS can be used as an effective ARC for textured or non-textured mc-Si solar cells with a very large area (100–164 cm^2). Moreover, stain etching can be used for selective emitter formation and passivation followed by screenprinted TiO_2 ARC deposition. The efficiency of 12–13% on an emitter, which is

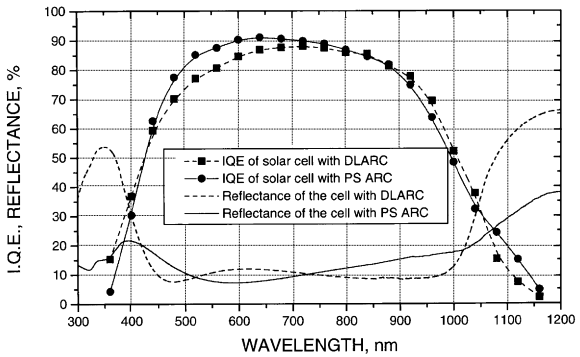

Fig. 20. IQE and reflectance characteristics of the cells with PS and double layer (TiO_2/MgF_2) ARC.

not yet optimized for PS formation, shows the large potential of stain etched PS in industrial mc-Si solar cells.

3.3.2. Electrochemical method

The electrochemical method allows to control the most important parameters of PS (thickness and porosity) through the use of an additional variable, the current density, which is a key formation parameter for the determination of the PS porosity. It allows to produce a very good ARC PS layer in less than 4 s so that PS layers in the emitter of n^+-p junctions can be formed without masking and damaging the industrial Ag screenprinted electrical front contact grid.

3.3.2.1. Experimental. The electrochemical method is applied by IMEC and CNRS-LPSB. The efficiency potential of a PS ARC is investigated by IMEC on high-quality FZ Si substrates ($2 \times 2\,cm^2$) having a P_2O_5-diffused emitter and evaporated Ti–Pd–Ag contacts. CNRS-LPSB focuses on the formation of a PS ARC for commercial mc-Si solar cells. $5 \times 5\,cm^2$ solar cells are made on NAOH textured n^+-p multicrystalline silicon (POLIX) junctions with a 0.3 μm $POCL_3$ diffused emitter. The Al and Ag electrical back and front contacts, respectively, are deposited by screen printing (followed by an annealing) as a routine industrial process developed at Photowatt Int. Company. Because of the Ag front contact is sensitive to the presence of HF, the PS layer is formed under galvanostatic conditions with a $50\,mA/cm^2$ constant current applied during 3.5 s. At the surface of the emitter, under the Ag electrical fingers, the P doping concentration is larger than 5×10^{20} atom/cm^3 and the sheet resistance is 25 Ω/□. This emitter is transformed into a 125 Ω/□ at the PS/bulk interface with the *P* concentration decreasing around 10^{19} atom/cm^3 [45]. From a spectroscopic ellipsometry study it is found that the thickness of the PS layer is 105 nm and a porosity gradient (60% porosity near the PS/bulk Si interface and 85% porosity near the PS surface) existed within the PS layer [46]. Previously to the PS formation, the wafers are NaOH chemically etched which leads to a new surface microstructure whose morphology depends on the crystallographic orientation of the

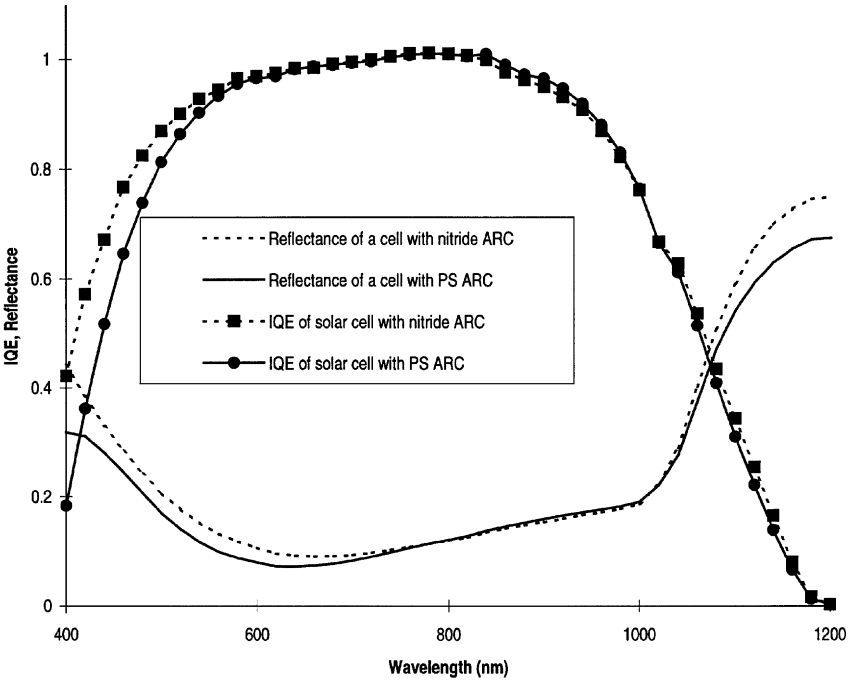

Fig. 21. IQE and reflectance characteristics of mono-Si cells with PS ARC and with conventional SiN ARC.

grains. The influence of the PS layer on the photovoltaic properties of the junction is investigated with respect to the crystallographic orientation of specific grains in the multicrystalline silicon wafer used [20]. It should be mentioned that the PS layer formation conditions used in this study are not those which lead to a PS layer with optical properties optimized for photovoltaic applications (see Fig. 3) [14,15], because the conditions of PS formation are drastically limited by the thickness of the junction and the presence of the front contact grid.

3.3.2.2. Results. The IQE of a cell with an optimized PS ARC and with a silicon nitride ARC are shown in Fig. 21. It is clearly seen that a similar reflectivity is obtained for PS and for the conventional SiN ARC. Due to the minimum in reflectance at 680 nm [34] the EQE reaches a maximal value of 0,87 at 680 nm, which represent a gain of 25% compared to the cell without a PS layer. Illuminated I–V analysis reveals that the solar cell efficiency strongly depends on the PS layer thickness because a small variation in ARC layer thickness (< 15 nm) affects the reflectance which in its turn results in a different J_{sc}. This effect is less pronounced on a textured surface. From Table 5 it can be concluded that applying a conventional electrochemical PS layer on an alkaline textured surface results in a higher J_{sc} and efficiency as compared to the non-textured case. The V_{oc} (605 mV) is similar to the

Table 5
PV output parameters of textured and non-textured FZ Si solar cells with an electrochemically formed PS surface layer as independently confirmed by NREL

Solar cell	J_{sc} (mA/cm^2)	V_{oc} (mV)	FF	EFF (%)
PS on non-textured cell	30.4	603	0.78	14.3
PS on textured cell	31.3	601	0.78	14.6

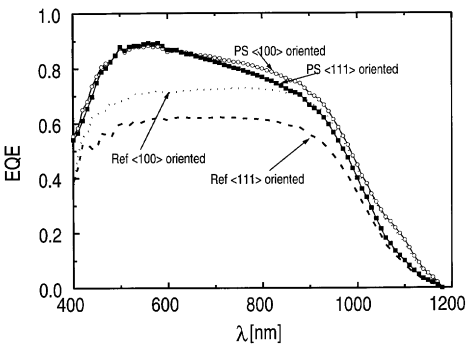

Fig. 22. EQE as a function of wavelength measured on the two ⟨1 0 0⟩ and ⟨1 1 1⟩ oriented grains of an n^+-p mc-Si junction without a PS layer (Ref) and with a PS layer (PS).

value which is obtained on high quality multicrystalline Si material (Section 3.2.4). This indicates that in both cases using a rather deep emitter leads to a V_{oc} which is not strongly affected by the PS surface layer.

The EQE of the two grains with PS and without (Ref) a PS layer are shown in Fig. 22. An increase in the spectral response is observed for the junctions with a PS layer compared to the reference junctions. The theoretical J_{sc} of two grains under AM 1.5 standard conditions, in the range 400–1100 nm, are calculated from the spectral response integrated between 400 and 1100 nm, according to the following equation:

$$J = q\int_{400}^{1100} \mathrm{EQE}(\lambda)J_0(\lambda)\mathrm{d}\lambda,$$

where q is the electron charge. Increases in I_{sc} of 16% and 30% are observed for ⟨1 0 0⟩ and ⟨1 1 1⟩ grains, respectively, after formation of a PS layer (Table 6).

In order to separate the modified reflectivity of the PS layer from other effects such as a light diffusing behaviour or surface passivation, the IQE = EQE/(1 − R) corresponding to Fig. 22 is plotted in Fig. 23. After correction for light absorption in the PS layer, the IQE of the reference for the ⟨1 0 0⟩ grain is lowered over the entire wavelength range compared to the PS n^+-p junction. This means that the change in

Table 6
Theoretical short circuit current for the ⟨1 0 0⟩ and ⟨1 1 1⟩ grains with and without a PS layer

	⟨1 0 0⟩ oriented grain		⟨1 1 1⟩ oriented grain	
	Ref	With a PS layer	Ref	With a PS layer
Theoretical J_{sc} (mA/cm^2)	22.7	26.3	19.2	25.5

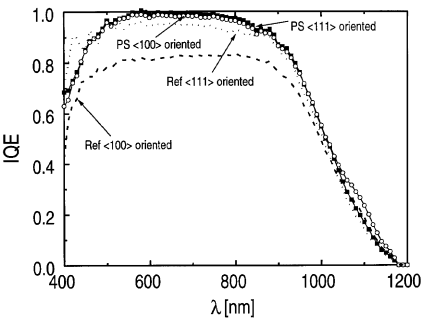

Fig. 23. IQE of the ⟨1 0 0⟩ and ⟨1 1 1⟩ grains corresponding to Fig. 22.

the reflectivity of the PS layer is not the only effect which determines the photoresponse after formation of a PS layer. For the ⟨1 1 1⟩ grain, the IQE is reduced in the short wavelength region after the PS formation. A slight increase of the IQE is also observed between 500 and 1000 nm for the ⟨1 1 1⟩ grain after PS treatment. In both cases the increase of the IQE of the grains with the PS layer is understood from the light scattering action of porous silicon, resulting in a higher collection efficiency.

The I–V curves under white light illumination are obtained from the whole area (5×5 cm^2) of the n$^+$/p junctions with and without a PS layer. A 20% increase in the photocurrent of the junction with the PS layer is observed, while the open circuit voltage V_{oc} was not modified. These results point to an increase of the fill factor [20]. The photovoltaic characteristics of the junction with the porous emitter, measured (by the solar cell manufacturer Photowatt Inc.) using the standard procedure are reported in Table 6 and compared to the characteristics of a conventional solar cell (NaOH textured and with a $SiO_2 + TiO_2$ double layer ARC). The characteristics of the cell with the PS layer (Eff = 13.2%) [20] are very similar to those of the chosen commercial cell whose characteristics are among the best produced by the company. Slight decreases in I_{sc} (3.8%) and V_{oc} (2%) are noticed for the PS n$^+$/p junction, whereas an increase in the fill factor (2.3%) is observed Table 7.

An efficiency of 13.2% on 25 cm^2 multicrystalline silicon solar cells with a porous Si selective emitter can be obtained using the regular industrial processing for making

Table 7
PV output parameters of a commercial Polix mc-Si solar cell and a 5×5 cm^2 Polix mc-Si solar cell with an electrochemically made PS selective emitter

Solar cell	J_{sc} (mA)	V_{oc} (mV)	FF	EFF (%)
Commercial cell	790	595	0.725	13.6
With PS layer	760	583	0.742	13.2

the n^+/p junctions and the front and back screenprinted contacts [20]. The electrochemical method leads to the formation of an efficient ARC PS layer between the Ag screenprinted fingers. Although being directly in contact with the corrosive HF solution, the front contact grid is not damaged, because the formation time is extremely short (< 4 s). The beneficial effect of a PS layer is more important for the grains whose crystallographic orientation does not favour the formation of surface pyramids during the NaOH texturization treatment of silicon.

4. Conclusion

It is shown that PS has a large potential in photovoltaics. A PS ARC acts as a perfect light diffusor and provides an appropriate reflectance which is quite comparable to the reflectance of a textured Si surface covered by conventional ARC. Moreover PS has some passivating capabilities, that allow to fabricate solar cells without an additional passivation coating. All these PS properties significantly simplify the solar cell processing.

The optimization of a selective emitter formation using PS etching results in a 14.1% efficiency mc-Si cell processed without texturization, surface passivation or additional ARC deposition. The implementation of a PS ARC into an industrially compatible screen-printed solar cell process is made by both chemical and electrochemical methods of PS formation. An efficiency of 13.2% is achieved for (25 cm^2) mc-Si solar cell using electrochemical technique while values between 12% and 13% are reached for very large (100–164 cm^2) commercial mc-Si cells by chemical method of PS formation. All results clearly indicate that 14–15% efficiency could be achieved by a very simple solar cell technology if all processing steps (PS formation, diffusion, metallization) will be fully optimized.

Further research on the topic of cost-effective mc-Si solar cells with PS selective emitter should be made in a way of further improving the optical, structural and surface-passivation characteristics of PS. Two possible ways are clearly visible at this moment. The first one is the fabrication of PS with a porosity gradient that provides both excellent reflectance and passivation. The second is the improvement of PS characteristics by external treatments such as: hydrogenation, etc. Both pathways are currently under investigation and intermediate results show interesting perspectives.

Acknowledgements

The authors strongly appreciate the help of the following persons: Dr. H. Bender (IMEC) and A. Parisini (CNR-LAMEL) for TEM-analysis, Dr. T Conard (IMEC) for XPS-analysis, W. Schmidt and F. Schomann (ASE GmbH) for wafer and cell delivering, P. De Schepper (IMEC), W. Laureys (IMEC) and H. Lautenschlager (ISE) for technical assistance, M. Montecchi (ENEA-Casaccia) for reflectance and E. Schäffer (ISE) for photovoltaic measurements. L. Stalmans acknowledges the support from IWT (Flemish Institute for Promotion of Scientific-Technological Research in the Industry). Part of this work was funded within the frame of the following programs: European Joule-III BANSIS-project (contract number: JOR3-CT96-0109), a CEE Contract (JOR3-CT95-0608) and the CNRS-ECODEV and ADEME through their photovoltaic program.

References

[1] J. Coppye, E. Demesmaeker, H.E. Elgamel, J. Szlufcik, M. Ghannam, J. Nijs, R. Mertens, D. Sarti, P. Loubly, Proceedings of the 10th EC Photovoltaic Solar Energy Conference, 1991, pp. 657–660.
[2] J. Szlufcik, H.E. Elgamel, M. Ghannam, J. Nijs, R. Mertens, Appl. Phys. Lett. 59 (1991) 1583.
[3] D.S. Ruby, P. Yang, M. Roy, S. Narayanan, Proceeding of the 26th IEEE Photovoltaic Specialists Conference, 1997, pp. 39–42.
[4] P. Menna, G. Di Francia, V. La Ferrara, Sol. Energy Matter. Sol. Cells 37 (1995) 13.
[5] S. Bastide, M. Cuniot, P. Williams, L.Q. Nam, D. Sarti, C. Lévy-Clément, Proceedings of the 12th EC Photovoltaic Solar Energy Conference, 1994, pp. 780–783.
[6] Y.S. Tsu, Y. Xiao, M.J. Heben, X. Wu, F.J. Pern, S.K. Deb, Proceedings of the 23rd IEEE Photovoltaic Specialists Conference, 1993, pp. 287–293.
[7] C. Lévy-Clément, A. Lagoubi, M. Neumann-Spallart, M. Rodot, R. Tenne, J. Electrochem. Soc. 138 (1991) 67–71.
[8] A. Prasad, S. Balakrishnan, S.K. Jain, G.C. Jain, J. Electrochem. Soc. 129 (1982) 596.
[9] G. Smestad, M. Kunst, C. Vial, Sol. Energy Matter. Sol. Cells 26 (1992) 277.
[10] Y.S. Tsuo, M.J. Heben, X. Wu, Y. Xiao, C.A. Moore, P. Verlinden, S.K. Deb, Proceedings of the MRS Symposium, Vol. 283, 1993, pp. 405–410.
[11] G.P. Wei, Y.M. Zheng, Z.J. Huang, Y. Li, J. Feng, Y.W. Mo, Sol. Energy Matter. Sol. Cells 35 (1994) 319–324.
[12] S.M. Vernon, N.M. Kalkhoran, H.P. Maruska, W.D. Halverson, Proceedings of the 1st World Conference. Photovoltaic Energy Conversion on 1994, 1583.
[13] L. Schirone, G. Sotgiu, F. Rallo, F.P. Califano, Proceedings of the 13th EC Photovoltaic Solar Energy Conference, 1995, 2447–2450.
[14] S. Bastide, S. Strehlke, M. Cuniot, A. Boutry-Forveille, Q.N. Le, D. Sarti, C. Lévy-Clément, Proceedings of the 13th EC Photovoltaic Solar Energy Conference, 1995, 1280.
[15] E. Vazsonyi, M. Fried, T. Lohner, M. Adam, T. Mohacsy, I. Barsony, J. Szlufcik, F. Duerinckx, J. Nijs, Proceedings of the 13th EC Photovoltaic Solar Energy Conference, 37–40.
[16] D.R. Turner, J. Electrochem. Soc. 105 (1958) 402.
[17] R.J. Archer, J. Phys. Chem. Solids 14 (1960) 14.
[18] L. Canham, Properties of Porous Silicon, UK, INSPEC, 1997, p. 405
[19] H. Bender, L. Stalmans, S. Jin, J. Poortmans, W. Vandervorst, J. Nijs, Appl. Surf. Science 147 (1999) 187.
[20] S. Strehlke, Q.N. Le, D. Sarti, A. Krotkus, K. Grigoras, C. Lévy-Clément, Thin Solid Films 297 (1997) 291.

[21] S. Strehlke, S. Bastide, C. Lévy-Clément, Solar Energy Materials and Solar Cells 57 (1999) 393.
[22] S. Shih, K.H. Jung, T.Y. Hsieh, J. Sarathy, J.C. Campbell, D.L. Kwong, Appl. Phys. Lett. 60 (1992) 1863.
[23] K.H. Jung, S. Shih, D.L. Kwong, J. Electrochem. Soc. 140 (1993) 3046.
[24] L. Schirone, G. Sotgiu, M. Montecchi, Journal of Luminescence 80 (1999) 163.
[25] L. Schirone, G. Sotgiu, M. Montecchi, Abstracts First Porous Semiconductors — Science and Technical Conference, 1998, p. 256.
[26] R.R. Bilyalov, H. Lautenschlager, C. Schetter, F. Schomann, U. Schubert, R. Schindler, Proceedings of the 14th EC Photovoltaic Sol. Energy Conference, 1997, pp. 788–791.
[27] L. Stalmans, J. Poortmans, H. Bender, M. Caymax, K. Said, E. Vazsonyi, J. Nijs, R. Mertens, Progr. Photovolt. 6 (1998) 233–246.
[28] A. A. Abouelsaood, M. Y. Ghannam, J. Nijs, Proceedings of the Second World Conference on Photovoltaic Energy Conversion, 1998, pp. 176–179.
[29] L. Stalmans, Ph.D. Thesis, Katholieke Universiteit Leuven, 1999.
[30] R.R. Bilyalov, H. Lautenschlager, R. Schindler, Proceedings of the Second World Conference on Photovoltaic Energy Conversion, 1998, pp. 1642–1645.
[31] L. Schirone, unpublished.
[32] L. Stalmans, J. Poortmans, H. Bender, S. Jin, T. Conard, L. Debarge, A. Slaoui, J. Nijs, Abstracts of the First Porous Semiconductors — Science and Technical Conference, 1998, pp. 30–31.
[33] S. Strehlke, S. Bastide, L. Stalmans, J. Poortmans, L. Debarge, A. Slaoui, C. Lévy-Clément, Proceedings of the Second World Conference on Photovoltaic Energy Conversion, 1998, pp. 1634–1637.
[34] S. Strehlke, D. Sarti, A. Krotkus, O. Polgar, M. Fried, J.P. Roger, C. Lévy-Clément, Proceedings of the 14th EC Photovoltaic Solar Energy Conference, 1997, pp. 2480–2484.
[35] L. Schirone, G. Sotgiu, M. Montecchi, A. Parisini, Proceedings of the 14th EC Photovoltaic Solar Energy Conference, 1997, pp. 1479–1482.
[36] A. Krotkus, K. Grigoras, V. Pasebutas, I. Barsony, E. Vazsonyi, M. Fried, J. Szlufcik, J. Nijs, C. Lévy-Clément, Sol. Energy Matter. and Sol. Cells 45 (1997) 267–273.
[37] L. Stalmans et al., Procceeding sof the 14th EC Photovoltaic Solar Energy Conference, 1997, pp. 980–985.
[38] E.A. Ponomarev, S. Bastide, Q.N. Le, D. Sarti, C. Lévy-Clément, Proceedings of the 14th EC Photovoltaic Solar Energy Conference, 1997, pp. 804–808.
[39] R. Einhaus, J. Szlufcik, E. Vazsonyi, J. Nijs, R. Mertens, Proceedings of the 26th IEEE Photovoltaic Specialists Conference, 1997, pp. 167–170.
[40] R.R. Bilyalov, R. Lüdemann, German Patent Application, 1998.
[41] R.R. Bilyalov, Final Report for Alexander von Humboldt Foundation, AvH, Germany, 1997.
[42] R. Lüdemann, R.R. Bilyalov, C. Schetter, Proceedings of the 14th EC Photovoltaic Solar Energy Conference, 1997, pp. 780–783.
[43] L. Schirone, G. Sotgiu, M. Montecchi, G. Righini, R. Zanoni, Proceedings of the Second World Conference on Photovoltaic Energy Conversion, 1998, pp. 276–279.
[44] R.R. Bilyalov, B. Groh, H. Lautenschlager, R. Schindler, F. Schomann, Proceedings of the 26th IEEE Photovoltaic Specialists Conference, 1997, pp. 147–150.
[45] S. Strehlke, Ph.D. Thesis, University Paris VI, 1998.
[46] S. Strehlke, D. Sarti, O. Polgar, M. Fried, C. Lévy-Clément, Photoelectrochemistry, NJ, PV 97–20 (1997) 278.